Simulation of Rippled-Sand Synthetic Aperture Sonar Imagery

Shawn F. Johnson, *Member, IEEE* and Anthony P. Lyons, *Member, IEEE*

***Abstract*—Simulation of Synthetic Aperture Sonar (SAS) imagery is of growing interest for training of both human operators and the 'supervised learning' of computer-aided detection / computer-aided classification (CADCAC) systems. Synthetic Aperture Sonar (SAS) imagery is often characterized by a decidedly non-Rayleigh amplitude distribution, owing to its inherent high-resolution combined with speckle, induced by the coherent image formation process. Effective simulation of SAS imagery must be both visually and statistically realistic. The method presented here has been developed to simulate rippled-sand Sonar imagery at high-frequencies (i.e., on the order of 100 kHz), which accounts for non-symmetric ripple shape, sediment acoustic properties, Sonar to ripple orientation, system resolution, signal to noise ratio, and coherent imaging induced speckle. This numerical simulation method is computationally inexpensive, and compares well both visually and statistically with collected data over a wide range of orientation angles. Simulation methods are presented with validation against SAS imagery collected by the Naval Surface Warfare Center – Panama City Division.**

***Index Terms*—clutter, non-Rayleigh reverberation, simulation synthetic aperture sonar (SAS)**

I. Introduction

SIMULATION of synthetic aperture sonar (SAS) imagery is of growing interest for training of both human operators and the 'supervised learning' of computer-aided detection / computer-aided classification (CADCAC) systems. To avoid 'negative training,' simulated imagery must posses a sufficient degree of visual and statistical realism. SAS imagery is capable of resolving seafloor sand ripples, and often exhibits significantly non-Rayleigh image amplitude statistics owing to the small resolution cell. Specifically for the CADCAC process, visual realism is imperative because of the role of pattern recognition, while amplitude statistics impact the 'first response' energy detector stage.

In this work, a heuristic physics-based approach is presented for simulation of rippled-sand SAS imagery which is visually convincing, statistically accurate, and computationally inexpensive. The simulation methodology is given in Section II. Section III presents visual and statistical comparison to experimental data with discussion, and conclusions follow in Section IV.

Manuscript received July 14, 2010. This work was supported by the Office of Naval Research Grant N00014-10-1-0151 and Code 32, and the National Defense Science and Engineering Graduate Fellowship.

S. F. Johnson is with the Applied Physics Laboratory, Johns Hopkins University, Laurel, MD 20723-6099 USA (e-mail: Shawn.Johnson@jhuapl.edu).

A. P. Lyons is with the Applied Research Laboratory, Pennsylvania State University, State College, PA 16804 USA (e-mail: apl2@psu.edu).

II. Simulation Methodology

A. Overview

Generation of random surfaces, or more relevantly simulation of remote-sensing imagery, with correlations in two dimensions is a topic of significant interest, and non-trivial implementation. A significant body of work exists for related fields of simulating ocean surface waves for Synthetic Aperture Radar and computer vision / virtual reality (e.g. [1, 2]). A heuristic method (Fig. 1) has been developed for simulating high-resolution synthetic aperture beamformed reverberation from rippled-sand [3]. This method draws on prior work from several sources [4-8], but incorporates them in a unique manner which provides visual and statistical realism, in a computationally efficient manner (a large acoustic simulation of several million image pixels can be computed on the order of seconds). It is important to note that no statistical form of the output normalized envelope pdf is assumed *a priori*, and the statistics of the simulation comes only from individual assumptions and parameter selections made at each step of the process.

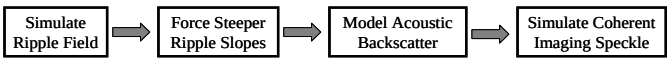

Fig. 1. Simulation steps for sand ripple image.

B. Ripple Generation

The method developed in this paper begins with the work of [8] which is used to generate a two-dimensional ripple field with non-fading characteristics (i.e., the ripple heights do not fade to the mean at bifurcation points). Fig. 2(a) shows a simulated ripple-field and corresponding two-dimensional wavenumber spectrum (Fig. 2(b)). A unique property of simulations based in the spatial frequency domain is that the resulting image is spatially-harmonic. Thus, a large surface can be generated by tiling several smaller surfaces without discontinuities at the junctions. The initial surface generated is symmetric with respect to zero mean height. That is, both the crests and troughs of the ripples are equidistant from the mean. Actual wave-generated sand ripples are rarely symmetric,

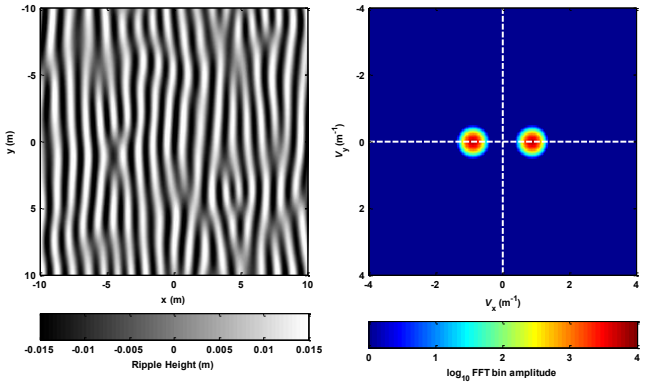

(a) (b)

Fig. 2. Simulated ripple field and corresponding two-dimensional wavenumber spectrum. $V_{x,y}$ represents spatial frequency with units of m^{-1}

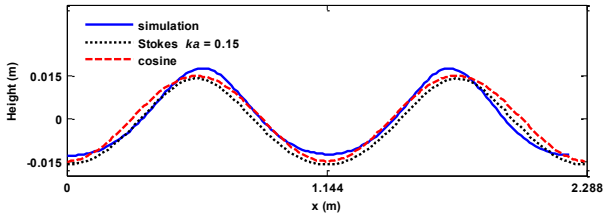

Fig. 3. Example realization of simulation (solid blue), Stokes ripple of Equation 1 with ka = 0.15 (solid black), and cosine (dashed red) of comparable wavelength.

often having a steeper slope with wider troughs and narrower crests. Lyons, et al. [9] show the height, h, of wave-generated sand ripples at position x can be closely approximated by a Stokes wave with three harmonics,

$$h(x) = -a\cos kx + \frac{1}{2}ka^2\cos 2kx - \frac{3}{8}k^2a^3\cos 3kx \quad (1)$$

where k is the spatial wavenumber and a is a parameter of the polynomial expansion, with $ka \approx 0.48$ (ka is based on the maximum steepness the medium can support, with $ka_{max} \approx 0.44$ assumed for sea-surface water ripples). An example Stokes wave with λ = 1.144 m (or k = 5.5 m^{-1}) and ka = 0.15 (resulting in less steepening than in [9]) is shown in Fig. 3, compared to a cosine of comparable period, and will serve as a benchmark. Implementation of the Stokes shape in the wavenumber domain for a random two-dimensional correlated surface requires generating harmonics and appropriately accounting for their phases. Steepened ripples can be implemented by rectifying the initial height-symmetric ripple field and filtering higher order harmonics [3] or by utilizing the exponential function of the vertically-symmetric surface multiplied by a skewness parameter while maintaining a zero mean and variance equal to the original surface [8]. The latter method is utilized for presentation here.

Fig. 3 shows a single realization of a simulated seafloor surface with skewness parameter b = 0.4 of [8] (Fig. 4(a)), and Fig. 5 shows the corresponding height histogram clearly depicting the desired height asymmetry. For comparison, the harmonics of Stokes wave with $ka \approx 0.15$ are compared to the

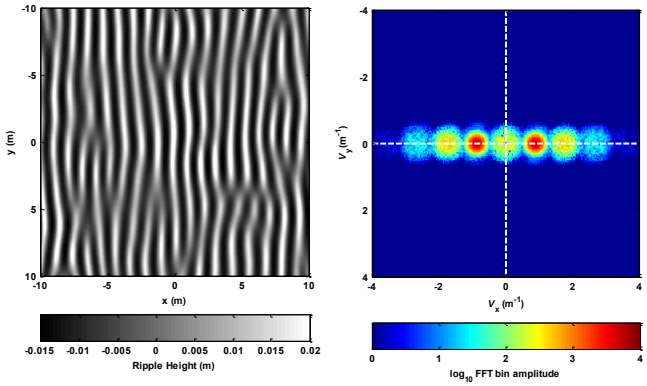

(a) (b)

Fig. 4. Simulated ripple field (note asymmetric color axis) and corresponding two-dimensional wavenumber spectrum after skewing process.

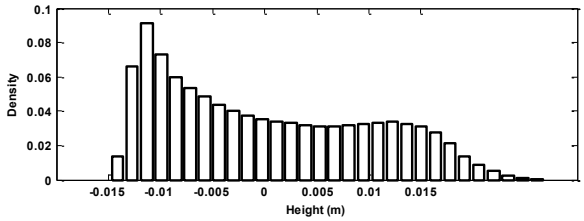

Fig. 5. Histogram of entire simulated surface after skewing (as in Fig. 4).

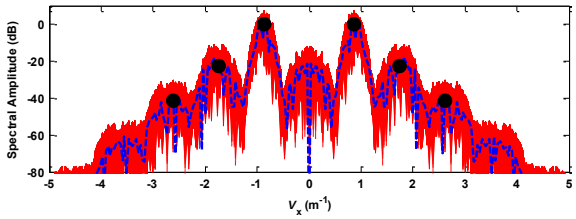

Fig. 6. Spatial Fourier Transform for 2048 iterations of surface (solid red), median value (dashed blue), and harmonics of Stokes wave (solid black dot). Harmonics of Stokes

median spectrum of 2048 realizations of the ripple field (Fig. 6) (note, Fourier Transforms are computed along the x-axis). These figures are in good agreement to data presented in [9] for observed wave-generated sand ripples.

C. Acoustic Response

At this point, it is assumed the backscattered acoustic energy of each image pixel is primarily determined by the average slope of the seafloor within the corresponding Sonar resolution cell (determined in II.C.) with respect to the backscattered direction (this assumption is valid for high-frequency systems which have a narrow horizontal beam-pattern, often only a few degrees). This slope is simply the change in height between pixels along the range dimension with respect to range including the grazing angle to the Sonar, which is typically on the order of 10 degrees or less for high-contrast SAS images [10]. The acoustic response of each Sonar resolution cell is then estimated using a polynomial expansion fit to the rough surface backscattering model of [4, 5, 7] (which is a combination of the small-roughness perturbation method for low grazing angles and the Kirchoff or tangent-plane approximation for near-normal grazing) for

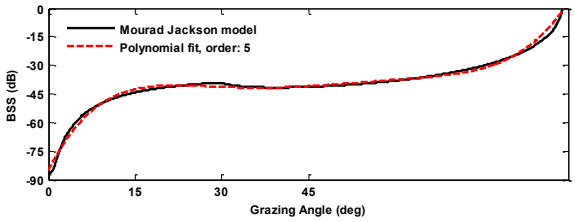

Fig. 7. Rough surface backscattering model of [4, 5, 7] (solid black) and 5th order polynomial fit used in simulation (dashed red).

computational speed. For the simulations here, the modeled acoustic response was based on the sand properties given in [7, 11, 12] and summarized in Table 1, approximated with a 5th order polynomial (Fig. 7). A much higher order polynomial (about 20th order for this case) would be required to capture the structure of the critical angle seen in the model, significantly increasing the computation time. It can be argued such a clearly defined critical angle is rarely seen in experimental backscattered acoustic data. A signal to noise ratio (SNR) is then specified by adding Gaussian distributed 'white' noise to simulate background environmental and system noise.

TABLE 1: SEDIMENT PROPERTIES USED IN SIMULATIONS.

Property		Value
Sediment / Water Density Ratio	ρ	2.00
Sediment / Water Sound Velocity Ratio	v	1.16
Attenuation	δ	0.01
Power Law Exponent	$\gamma 2$	3.04
Power Law Spectral Strength	$w2$	4.33×10^{-5}

D. Simulating Speckle

The final step is to simulate speckle phenomena, which is well documented in the optics and radar literature, with a few references for speckle mitigation in SAS images [13, 14]. Speckle is the result of constructive and destructive interference of the wavefronts scattered by a rough surface, and the resulting imagery bears no relationship to the macroscopic properties of the ensonified surface [15]. Speckle is clearly superimposed on the rippled-sand imagery from experimental SAS data (Fig. 8). This interference pattern is the result of random phase perturbations of the wavefronts from individual scatters within the resolution cell which are superimposed during the coherent imaging process [16, 17]. Calculation of the autocorrelation coefficients in both the along-track (i.e., parallel to ripple crests) and slant-range (i.e., perpendicular to ripple crests) shows de-correlation after 1-2 resolution cells consistent with [18]. Goodman [6] gives a simple algorithm for generating speckle (Fig. 9). This method utilizes the inverse Fourier transform of a two-dimensional random phase spectra (a similar method is presented in [19] for simulating diffraction patterns by specifying the amplitudes and speckle patterns by specifying the random phases of an inverse Fourier transform). When the speckle process is driven by a second compounding random process, the resulting phenomenon can be considered 'compound' speckle and has been shown to lead to the *K* distribution [6, 20]. This second random process (roughness of the scattering surface being the first), can be the result of a turbulent medium or errors in platform motion compensation. It is also hypothesized that a second order scattering feature (e.g. sand-dollars on rippled-sand) may also produce something resembling compound speckle, however this requires additional consideration and validation with experimental data. Speckle observed in the SAS image of Fig. 8 have greater distance between peaks than Fig. 9(a), and appear more like the compound speckle of Fig. 9(b). For these reasons, compound speckles produced by two independent realizations multiplied together, are used for this simulation. The acoustic response of the sand ripples simulated previously is then multiplied by this compound speckle to produce the final image.

III. COMPARISON TO COLLECTED DATA AND DISCUSSION

A. Experimental Data Overview

Data presented here come from the Small Synthetic Aperture Minehunter (SSAM), a joint development between the Naval Surface Warfare Center – Panama City Division and the Applied Research Lab – Penn State. SSAM is a REMUS 600 Autonomous Underwater Vehicle (AUV) based Sonar suitable for synthetic aperture processing. Data were provided as complex beamformed and motion compensated images, and come from demonstration experiments near La Spezia, Italy and Panama City, FL, USA. The images presented here have a resolution of $\Delta x_{slant} \approx 5.8$ cm by $\Delta y_{SAS} \approx 2.0$ cm corresponding to slant-range and along-track respectively, and collected at a center frequency of 120 kHz. A more complete description of the experiments conducted with, and development of, the SSAM system can be found in [21-26].

B. Visual Comparison

Figs. 10-12 show both simulated and collected rippled-sand SAS imagery for a variety of along-track to ripple crest orientation angles $\Psi = 6°, 69°, \& 86°$ with an average grazing angle at the center of each image of 10°. For all angles presented, once seafloor and Sonar parameters are appropriately specified for the simulation, good agreement is observed with collected data.

C. Statistical Comparison

To compare statistical realism of the images, several pre-processing steps are required. These steps involve decimation at the spatial bandwidth in both the slant-range and along-track dimensions, and normalization to remove gross power fluctuations while retaining the small-scale structure of the data. The normalization processes employed here is a two-dimensional constant False Alarm rate (CFAR) normalizer.

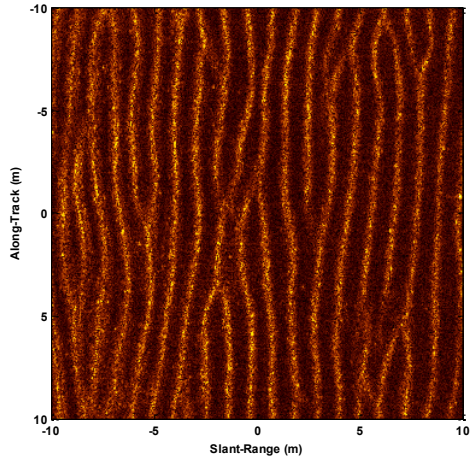

Fig. 8. Experimental rippled-sand SAS imagery showing acoustic response with coherent imaging speckle superimposed.

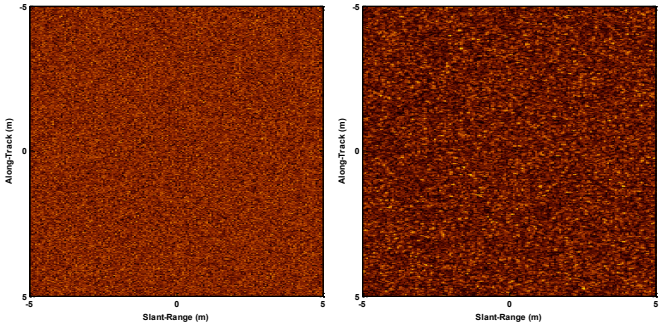

(a) (b)

Fig. 9. Comparison of single speckle (a) versus compound speckle (b), both with unit mean intensity.

This technique is implemented by creating a smoothed two-dimensional version of the data matrix, which has the dimension of along-track pings (or synthetic aperture) by slant-range samples. The filter window has variable width and guard band distances in both directions which are set by the user, and the mean intensity of the data contained within that window is computed; the resulting normalization surface is then applied to the data resulting in a smoothed version corresponding to the mean power fluctuations underlying the data surface. The original complex data are then divided by the amplitude of this smoothed version. Additional details can be found in [3, 27, 28]**.** Figs. 13 & 14 shows a comparison of the probability density function (pdf) for normalized experimental and simulated data, compared to the Rayleigh distribution.

D. Discussion

In general, the simulation provides good agreement both visually and statistically with the experimental results. As with any simulation, realism depends upon both the ability of the model to capture the physics, but also the appropriate parameter selection. For the simulations presented here, parameter values were obtained from direct or historic measurements (e.g. sediment properties, ripple wavelength), however some 'tuning' is required by the user for other

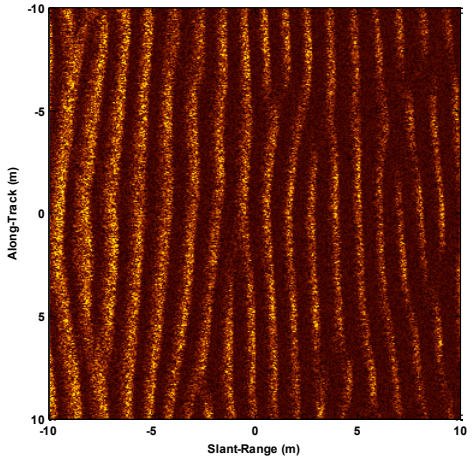

Fig. 10. Simulated imagery corresponding to Fig. 8, with Ψ = ~ 0 and λ = 1.14 m.

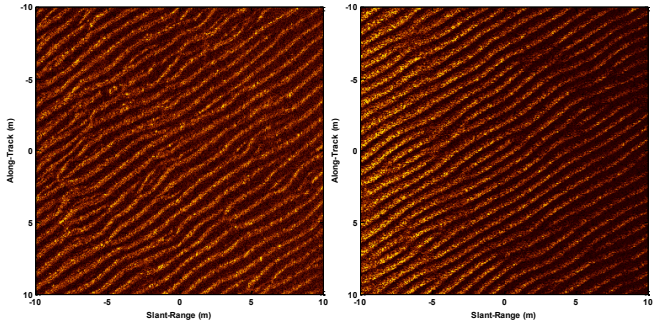

(a) (b)

Fig. 11. Experimental imagery (a) and simulated image (b), with Ψ = ~ 70 and λ = 0.76 m.

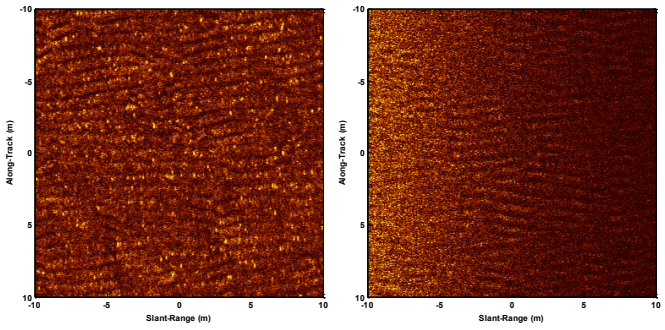

(a) (b)

Fig. 12. Experimental imagery (a) and simulated image (b), with Ψ ~ 90 and λ = 0.76 m.

parameters (e.g. ripple skewness, signal-to-noise ratio). Direct measurements of these parameters should further improve agreement.

The most noticeable visual difference between experiment and simulation occurs when the angle between the along-track dimension and ripple crest approaches perpendicular (Ψ ~ 90°). At this angle, the local acoustic slope variance is minimized and thereby the acoustic backscatter variance, resulting in a reduction in contract of the ripples. Careful examination of the experimental image (Fig. 12(a)) reveal at this orientation, additional strong 'speckles' appear in between the ripple crests. Recalling Section II-*D*, a compound

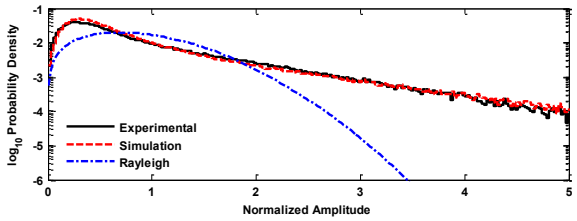

Fig. 13. Comparison of pdf's for experimental imagery of Fig. 8 (solid black) versus simulated imagery of Fig. 10 (dashed red) with $\Psi \sim 0°$ and $\lambda = 1.14$ m. Also shown is the Rayleigh distribution (dot-dashed blue).

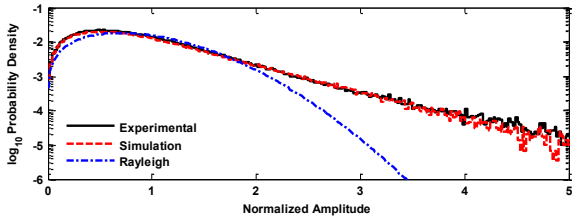

Fig. 14. As Fig. 13, for experimental imagery of Fig. 12(a) (solid black) versus simulated imagery of Fig. 12(b) (dashed red) with $\Psi \sim 90°$ and $\lambda = 0.76$ m.

representation of multiplicative speckle was applied during the simulation of images. While this is a common method to simulate speckle [6], it drives the placement of speckles to locations where the image has a non-zero value, notably along the ripple crests which have higher acoustic backscattering than the troughs. While the spacing between the simulated speckles appears similar to experimental speckle, the experimental speckle persists in the troughs particularly for the perpendicular case, thus causing the experimental data to have a different appearance. Analysis of image speckle with corresponding ground truth to confirm or deny presence of sediment inhomogeneties or biological source (e.g. shell fragments or sand dollars) is required to proceed. Despite a difference in the placement of speckle, the agreement between experimental and simulated statistical results is striking.

IV. Conclusions

Although numerous techniques have been proposed, the problem of generating physics-based synthetic data continues to plague the Radar and Sonar communities. With the increased use of computer-aided detection and classification systems to help mitigate high data rates and increased Probability of False Alarms caused by higher system resolutions, and an inability to collect training data for every sort of environment encountered, realistic simulation of cluttered reverberation is of paramount importance. This work has introduced a new method for simulating SAS images from rippled-sand which takes into account Sonar system parameters, sediment characteristics, and orientation to the sea-floor to produce synthetic acoustic imagery which agree both visually and statistically with experimental data in a computationally efficient manner.

It is anticipated that the method outlined in this paper for simulation of a rippled-sand SAS image can be expanded to incorporate alternative scattering mechanisms such as volume scattering or sediment inhomogeneties by modifying the backscattering model or with additional steps. Additionally, this method may be expanded to model specific system beampattern and beamforming techniques, and system specific speckle properties. These extensions require additional investigation.

Acknowledgment

The authors acknowledge the assistance, comments, and suggestions from the following during the scope of this research: Doug Abraham (CausaSci, LLC), Kerry Commander (NSWC-PC), DJ Tang (APL-UW), Kevin Williams (APL-UW), Dan Brown (ARL-PSU), J. Tory Cobb (NSWC-PC), and Jason Stack (ONR).

References

[1] F. Nouguier, C.-A. Guérin, and B. Chapron, "'Choppy wave' model for non-linear gravity waves," *Journal of Geophysical Research - Oceans*, vol. 114, pp. 1-16, 2009.

[2] J. Fréchot, "Realistic simulation of ocean sufrace using wave spectra," *Journal of Virtual Reality and Broadcasting*, vol. 4, December 2007.

[3] S. F. Johnson, "Synthetic aperture sonar image statistics," Ph.D. dissertation, Acoustics, The Pennsylvania State University, State College, Pennsylvania, 2009.

[4] P. D. Mourad and D. R. Jackson, "High-frequency sonar equation models for bottom backscatter and forward loss," presented at the Oceans 1989, 1989.

[5] P. D. Mourad and D. R. Jackson, "A model/data comparison for low-frequency bottom backscatter," *J. Acoust. Soc. Am.*, vol. 94, pp. 344-358, Jul 1993.

[6] J. W. Goodman, *Speckle Phenomena in Optics, Theory and Applications*. Englewood: Roberts & Company, 2007.

[7] D. R. Jackson, M. D. Richardson, *High-Frequency Seafloor Acoustics*. New York: Springer, 2007.

[8] D. Tang, F. S. Henyey, B. T. Hefner, and P. A. Traykovski, "Simulating realistic-looking sediment ripple fields," *IEEE J. Ocean. Eng.*, vol. 34, pp. 444-450, October 2009.

[9] A. P. Lyons, W. L. J. Fox, T. Hasiotis, and E. Pouliquen, "Characterization of the two-dimensional roughness of wave-rippled sea floors using digital photogrammetry," *IEEE J. Ocean. Eng.*, vol. 27, pp. 515-524, July 2002.

[10] A. P. Lyons, D. A. Abraham, and S. F. Johnson, "Modeling the effect of seafloor ripples on synthetic aperture sonar speckle statistics," *IEEE J. Ocean. Eng.*, vol. 35, pp. 242-249, April 2010.

[11] M. D. Richardson, K. B. Briggs, L. D. Bibee, P. A. Jumars, W. S. Sawyer, D. B. Albert, R. H. Bennett, T. K. Berger, M. J. Buckingham, N. P. Chotiros, P. H. Dahl, N. T. Dewitt, P. Fleischer, R. Flood, C. F. Greenlaw, D. V. Holliday, M. H. Hulbert, M. P. Hutnak, P. D. Jackson, J. S. Jaffee, H. P. Johnson, D. L. Lavoie, A. P. Lyons, C. S. Martens, D. E. McGehee, K. D. Moore, T. H. Orsi, J. N. Piper, R. I. Ray, A. H. Reed, R. F. L. Self, J. L. Schmidt, S. G. Schock, F. Simoney, R. D. Stoll, D. Tang, D. E. Thistle, E. I. Thorsos, D. J. Walter, and R. A. Wheatcroft, "Overview of SAX99: environmental considerations," *IEEE J. Ocean. Eng.*, vol. 26, pp. 26-53, January 2001.

[12] K. L. Williams, D. R. Jackson, E. I. Thorsos, D. Tang, and K. B. Briggs, "Acoustic backscattering experiments in a well characterized sand sediment: data/model comparisons using sediment fluid and biot models," *IEEE J. Ocean. Eng.*, vol. 27, pp. 376-387, July 2002.

[13] J. Chanussot, F. Maussang, and A. Hétet, "Scalar image processing filters for speckle reduction on synthetic aperture sonar images," presented at the Oceans 2002, 2002.

[14] S. A. Fortune, M. P. Hayes, and P. T. Gough, "Speckle reduction of synthetic aperture sonar images," presented at the World Congress on Ultrasonics 2003, Paris, France, 2003.

[15] J. W. Goodman, "Some fundamental properties of speckle," *J. Opt. Soc. Am.*, vol. 66, pp. 1145-1150, November 1976.

[16] J. W. Goodman, *Introduction to Fourier Optics*, 3rd ed. Englewood: Roberts & Company, 2005.
[17] J. W. Goodman, *Statistical Optics*. New York: Wiley, 2000.
[18] T. J. Skinner, "Surface texture effects in coherent imaging," *J. Opt. Soc. Am.*, vol. 53, p. 1350, 1963.
[19] F. Gascón and F. Salazar, "A simple method to simulate diffraction and speckle patterns with a PC," *Optick*, vol. 117, pp. 49-57, 2006.
[20] E. Jakeman and P. N. Pusey, "A model for non-Rayleigh sea echo," *IEEE Trans. Antennas Propogat.*, vol. 24, pp. 806-814, Nov. 1976.
[21] R. P. Stokey, A. Roup, C. von Alt, B. Allen, N. Forrester, T. Austin, R. Goldsborough, M. Purcell, F. Jaffre, G. Packard, and A. Kukulya, "Development of the REMUS 600 autonomous underwater vehicle," presented at the Oceans 2005, 2005.
[22] D. A. Cook, J. T. Christoff, and J. E. Fernandez, "Motion compensation of AUV-based synthetic aperture sonar," presented at the Oceans 2003, 2003.
[23] D. A. Cook, J. S. Stroud, J. E. Fernandez, and J. D. Lathrop, "Results from a hybrid synthetic aperture sonar motion estimation scheme," presented at the Oceans 2005 Europe, 2005.
[24] D. A. Cook, "Synthetic Aperture Sonar motion estimation and compensation," M.S. thesis, Electrical and Computer Engineering, Georgia Institute of Technology, 2007.
[25] J. E. Fernandez, A. D. Matthews, D. A. Cook, and J. S. Stroud, "Synthetic Aperture Sonar development for autonomous underwater vehicles," presented at the Oceans 2004, 2004.
[26] D. Brown, D. Cook, and J. Fernandez, "Results from a small Synthetic Aperture Sonar," presented at the Oceans 2006, 2006.
[27] S. F. Johnson, A. P. Lyons, and D. A. Abraham, "Bandwidth dependence of high-frequency seafloor backscatter statistics," presented at the Boundary Influences In High Frequency, Shallow Water Acoustics, University of Bath, UK, 2005.
[28] S. F. Johnson, A. P. Lyons, and D. A. Abraham, "Dependence of synthetic aperture sonar image statistics on resolution," presented at the International Symposium on Underwater Reverberation and Clutter, Lerici, Italy, 2008.

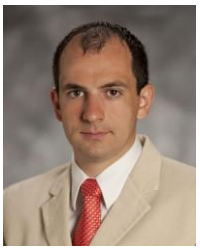

Shawn F. Johnson (S'04–M'09) received the B.M. degree in trombone performance, the B.M. degree in recording arts and sciences, and the M.A. degree in acoustics and audio from The Johns Hopkins University/Peabody Conservatory, Baltimore, MD, in 2001, 2002, and 2002, respectively, and the Ph.D. degree in acoustics from The Pennsylvania State University, State College, in 2009.

He is a Senior Research Physicist with the The Johns Hopkins University Applied Physics Laboratory, and Adjunct Professor of Acoustics with The Johns Hopkins University Peabody Conservatory. He was a Student Research Assistant at the NATO Undersea Research Centre, La Spezia, Italy, and was also a National Defense Science and Engineering Graduate and National Defense Industry Association Fellow.

Dr. Johnson is a full member of the Acoustical Society of America (ASA) and a member of the IEEE Oceanic Engineering Society.

Anthony P. Lyons (M'96) received the B.S. degree (*summa cum laude*) in physics from Henderson State University, Arkadelphia, AR, in 1988 and the M.S. and Ph.D. degrees in oceanography from Texas A&M University, College Station, in 1991 and 1995, respectively.

He was a Scientist at the SACLANT Undersea Research Centre from 1995 to 2000 where he was involved in a variety of projects in the area of environmental acoustics. Currently, he is a Senior Scientist at the Applied Research Laboratory, The Pennsylvania State University, State College, where he is engaged in studies of high-frequency shallow-water propagation, acoustics interaction with the seafloor, and high-resolution characterization of seafloor sediments.

Dr. Lyons was awarded, with the recommendation of the Acoustical Society of America, the Institute of Acoustics (U.K.) A.B. Wood Medal "for distinguished contributions in the underwater application of acoustics" in 2003. He is a Fellow of the Acoustical Society of America and a member of the IEEE Oceanic Engineering Society.